Phytopathology® · 2022 · 112:345-354 · https://doi.org/10.1094/PHYTO-03-21-0107-R

Molecular and Physiological Plant Pathology

e-Xtra*

Biochemical and Histological Insights into the Interaction Between the Canker Pathogen *Neofusicoccum parvum* and *Prunus dulcis*

Jerome Pouzoulet,[1] Daniel J. Yelle,[2] Bassam Theodory,[1] Eugene A. Nothnagel,[1] Sebastiaan Bol,[1] and Philippe E. Rolshausen[1,†]

[1] University of California, Department of Botany and Plant Sciences, Riverside, CA 92521
[2] USDA Forest Service, Forest Products Laboratory, Madison, WI 53726
Accepted for publication 14 July 2021.

ABSTRACT

The number of reports associated with wood dieback caused by fungi in the Botryosphaeriaceae in numerous perennial crops worldwide has significantly increased in the past years. In this study, we investigated the interactions between the canker pathogen *Neofusicoccum parvum* and the almond tree host (*Prunus dulcis*), with an emphasis on varietal resistance and host response at the cell wall biochemical and histological levels. Plant bioassays in a shaded house showed that among the four commonly planted commercial almond cultivars ('Butte', 'Carmel', 'Monterey', and 'Nonpareil'), there was no significant varietal difference with respect to resistance to the pathogen. Gummosis was triggered only by fungal infection, not by wounding. A two-dimensional nuclear magnetic resonance and liquid chromatography determination of cell wall polymers showed that infected almond trees differed significantly in their glycosyl and lignin composition compared with healthy, noninfected trees. Response to fungal infection involved a significant increase in lignin, a decrease in glucans, and an overall enrichment in other carbohydrates with a profile similar to those observed in gums. Histological observations revealed the presence of guaiacyl-rich cell wall reinforcements. Confocal microscopy suggested that *N. parvum* colonized mainly the lumina of xylem vessels and parenchyma cells, and to a lesser extent the gum ducts. We discuss the relevance of these findings in the context of the compartmentalization of decay in trees model in almond and its potential involvement in the vulnerability of the host toward fungal wood canker diseases.

Keywords: biochemistry and cell biology, disease resistance, endophytic interactions, fungal pathogens, host–parasite interactions

The fungal family Botryosphaeriaceae includes important generalist plant pathogens that have adapted to broad geographic range with diverse climatic conditions and a large spectrum of plant hosts (Batista et al. 2021; Slippers and Wingfield 2007). Infections by Botryosphaeriaceae pathogens typically result in the formation of wood cankers (also known as Bot cankers) that lead to dieback of the trunk, limb, and twig and eventually death of host. Over the last decade, the California tree crop industry has seen an increase of Bot canker outbreaks, notably on the almond tree *Prunus dulcis* L. (Holland et al. 2021; Moral et al. 2019b). It has been attributed to a combination of factors that include the intensification of agricultural practices and climate changes that are leading to favorable conditions for inoculum buildup and disease expression (Moral et al. 2019b). Comparable disease outbreaks attributed to the Botryosphaeriaceae have been reported globally on many hosts, such as grapevine, kiwi, citrus, and various nut crops, and have raised concerns about their potential impact on perennial cropping systems in the context of a changing climate (Adesemoye et al. 2014; Agustí-Brisach et al. 2020; Gramaje et al. 2016; López-Moral et al. 2020; Moral et al. 2019b; Olmo et al. 2016; Úrbez-Torres 2011; Zlatković et al. 2016).

Signs of infection by Botryosphaeriaceae fungi in almond trees often appear at the base of the tree trunk as a band of dead bark from which gum exudes, resulting in the common name "band canker" (Moral et al. 2019b). Necrotic lesions extending into the xylem tissue underneath the band of dead bark are also commonly observed. Band canker may be the result of growth cracks associated with vigorous trees and wounding caused by mechanical shakers, which become the point of entry for pathogens into woody tissue (Holland et al. 2021; Moral et al. 2019a). Infection can also occur through pruning wounds of lateral branches, leading to canopy canker. Infection of the trunk and scaffold branches causes chlorosis of leaves, wilting, and the gradual decline of the tree. The first description of the disease was established in the mid-1950s in California, and *Botryosphaeria dothidea* was identified as the causal agent two decades later (English et al. 1975). Since then, surveys and phylogenetic studies conducted in California and Spain have identified ≥11 species of Botryosphaeriaceae associated with cankers on almond trees (Holland et al. 2021; Inderbitzin et al. 2010; Olmo et al. 2016), and species of the genus *Neofusicoccum* were established as the most virulent pathogens (Holland et al. 2021; Inderbitzin et al. 2010). All commercial almond cultivars are susceptible to Bot canker disease, but previous studies indicated that contrasting levels of resistance could be found among almond cultivars and *Prunus* hybrids (English et al. 1975; Mancero-Castillo et al. 2018). For example, a recent study showed that the resistance to peach fungal gummosis caused by *B. dothidae* is under the control of inheritable genetic components in *Prunus* hybrids (Mancero-Castillo et al. 2018). Although almond cultivars probably differed in their ability to resist *B. dothidae* infection (English et al. 1975), information is lacking about the behavior of almond cultivars toward more aggressive Botryosphaeriaceae such as *Neofusicoccum parvum.*

Xylem is a complex and heterogeneous tissue in which the spatiotemporal structure of defenses plays a pivotal role in the ability

†Corresponding author: P. E. Rolshausen; philrols@ucr.edu

Funding: This research was funded by the U.S. Department of Agriculture (USDA), National Institute of Food and Agriculture, Specialty Crop Research Initiative (grant 2012-51181-19954). This study made use of the National Magnetic Resonance Facility at Madison, Wisconsin, which is supported by the National Institutes of Health (NIH), National Institute of General Medical Sciences grant P41GM103399, old number P41RR002301. Equipment was purchased with funds from the University of Wisconsin–Madison, the NIH (grants P41GM103399, S10RR02781, S10RR08438, S10RR023438, S10RR025062, and S10RR029220), the National Science Foundation (grants DMB-8415048, OIA-9977486, and BIR-9214394), and the USDA.

*The *e-*Xtra logo stands for "electronic extra" and indicates there are supplementary materials published online.

The author(s) declare no conflict of interest.

of the host to wall off microbial attacks and resist infections (Morris et al. 2020; Pearce 1996). The compartmentalization of decay in trees (CODIT) model illustrates how four different anatomical boundaries (referred to as walls) within the xylem could be used strategically to restrict the movement of pathogens in given spatial directions (Shigo 1984). Wall 1 aims to limit longitudinal movement of pathogens and is assured by the occlusion of xylem vessels by tyloses and gels. Wall 2 restricts the inward movement of pathogens and is provided by the growth ring boundary. Wall 3 impairs lateral movement of the pathogens, which is realized by ray parenchyma. Finally, wall 4 impedes outward movement of the pathogen and is provided by a modified layer of xylem produced in response to infection and injury. Wall 4 is sometimes regarded as the most important wall when it comes to host survival because it maintains vascular cambium integrity and retains the host's ability to regenerate functional secondary vascular tissues upon infection (Morris et al. 2020; Pearce 1996). In xylem parenchyma, the response observed at the cellular level can include the intracellular accumulation of antimicrobial compounds and structural modifications including thickening of the cell wall with lignin and suberin (Morris et al. 2020).

Pathogens causing wood cankers are necrotrophs and need to progress into their host to acquire carbon for their growth, which can be achieved through the digestion of cell wall materials (Cantu et al. 2008; Miedes et al. 2014; Rolshausen et al. 2008). Pathogens preferentially digest cell wall polysaccharides, and the highly recalcitrant nature of cell wall lignin, the biopolymer in which polysaccharides are embedded, makes xylem biodegradation heavily dependent on the chemistry of the cell walls (Miedes et al. 2014; Sattler and Funnell-Harris 2013). In connection with this concept, higher lignin content has been associated with higher resistance toward fungal pathogens (Martin et al. 2007; Miedes et al. 2014; Rolshausen et al. 2008). One should note the diversity in the CODIT response that occurs between and within perennial plant species (Morris et al. 2020; Pearce 1996). For example, species in the genus *Prunus* respond to xylem infection by forming gum ducts during the period of cambium activity (Bouaziz et al. 2016b). Although the genesis of gum ducts and the chemical composition of gum exudates have been documented (Biggs and Britton 1988; Bouaziz et al. 2016b), their potential role within the CODIT framework, along with other molecular and histological features of the xylem compartmentalization process in *Prunus*, has received little attention.

The overall aim of this study was to gain new insights in the interaction between the almond tree, *Prunus dulcis* L., and the canker pathogen *N. parvum*. First, we evaluated whether four almond cultivars exhibited contrasting levels of resistance upon experimental inoculation of the pathogen. Second, we characterized changes in the xylem cell wall chemistry triggered in response to infection and coupled these analyses with biochemical characterization of gum exudates. Finally, we complemented these data with a histological study to interpret these observations according to the CODIT framework.

MATERIALS AND METHODS

Evaluation of almond cultivars susceptibility to *N. parvum*. Evaluation of almond tree resistance to *N. parvum* was conducted on *Prunus dulcis* L. 'Butte', 'Carmel', 'Monterey', and 'Nonpareil' grafted on Lovell rootstock (Duarte Nursery Inc, Hughson, CA). Trees were trained with five branches and were grown in a shaded house at the University of California, Riverside, in 9.5-liter plastic pots containing a mix of compost and sand (1:1) and were watered daily. Soil was amended with controlled release fertilizer (Scotts Osmocote Classic, N:P:K 14:14:14, Marysville, OH), and trees received a foliar spray of Liquinox Iron and Zinc (Liquinox Co., Orange, CA) as specified by the manufacturers. A total of 160 plants were organized in two separate experiments (repetition A and B with 80 plants each), and each treatment (*N. parvum*-inoculated and mock-inoculated control plants) included 10 plants per cultivar (four cultivars × two treatments × 10 plants × two experiments = 160 plants). The two experimental repetitions were done at a 6-week interval at the end of the dormant season in 2017 (February and March 2017).

Resistance bioassays were performed in the main trunk as follows: 2-week-old culture of *N. parvum* voucher isolation UCD646so, grown on potato dextrose agar (PDA) medium at room temperature, was used as the inoculum. A piece of bark of 5 mm in diameter was removed from the stem with a cork borer (cleaned with ethanol and flamed) in order to expose the xylem. Inoculation proceeded about 10 cm bellow the top of the main trunk (see Supplementary Fig. S1). A PDA plug of fungal culture of the same size was introduced in the wound, with the mycelium facing the wound, and the site of infection was subsequently covered with Parafilm. Sterile PDA medium was used as mock control (i.e., wounded noninoculated trees). Trunks were cut and analyzed when visible canker from the outside (bark appeared black and sunken) reached approximately 30 mm in length for at least one of the cultivars (10 weeks after inoculation for repetition A and 6 weeks for repetition B). Trunks were cut longitudinally in the axis, streaking the inoculation site to expose both cankers (necrosis of phloem and cambium) and internal necrotic lesions (browning of the xylem vessels; see Supplementary Fig. S1). One half of the trunk was used for the histological analysis as described below. The other half was used for accurate measurements of internal necrotic lesions and cankers with a digital caliper, and the biochemical analyses of almond wood were performed as described below. The effects of cultivars, inoculation treatments on cankers, and necrotic lesion lengths were assessed via an analysis of variance (ANOVA) followed by pairwise comparisons of groups (Tukey HSD test) in R version 3.6.

Biochemical composition of almond wood cell walls after *N. parvum* infection. Wood samples from the in planta bioassays were used for these analyses. Wood fragments collected from the edge of the wound induced by the cork borer during inoculation to 20 mm above were stored at −80°C. On the transverse plane of the trunk, samples represented a quarter of the trunk (0 to 90° from the center of the inoculation wound). Bark layers of the almond tree stems were removed before sample preparation to leave only the xylem. Subsequently, samples were lyophilized for 48 h with a Labconco FreeZone 2.5 l freeze dryer (Kansas City, MO). For each cultivar, 10 almond tree xylem samples were pooled and were cut to pieces of approximately 3 mm. These samples (dry and chopped) were added to a Retsch (Haan, Germany) PM100 planetary ball mill equipped with a 50-ml ZrO_2 cup and ZrO_2 balls. The samples (approximately 200 mg) were milled with three 20-mm balls at 300 rpm for 80 min, with an interval of 20 min and pause time of 10 min between intervals, for a total of 60 min mill time. Then, the 20-mm balls were replaced by 10 10-mm balls and milled at 600 rpm for 260 min with a 20-min interval and 10-min pause, for a total of 180 min milling time. The wood dissolution method was similar to a previously described method (Lu and Ralph 2003). Briefly, ball-milled plant samples (100 mg) were added to 2 ml of dimethylsulfoxide and 1 ml of 1-methylimidazole, stirred overnight, acetylated in situ with 600 µl of acetic anhydride for 1.5 h, and precipitated quantitatively in 400 ml of water with stirring for 0.5 h. The settled precipitate was vacuum filtered with a Whatman nylon membrane having 0.2-µm pores, washed with 2 × 200 ml of distilled water, and dried in a 50°C vacuum oven.

Nuclear magnetic resonance (NMR) spectra were acquired on a 500-MHz Bruker–BioSpin (Rheinstetten, Germany) AVANCE spectrometer fitted with a cryogenically cooled 5-mm Bruker TCI gradient probe with inverse geometry (NMRFAM, University of Wisconsin, Madison, WI). Samples of acetylated material (60 mg) were analyzed in 500 µl of deuterochloroform ($CDCl_3$). Chemical shifts for lignin substructures were checked against authentic low molecular weight model compounds, by comparison with fully assigned spectra already in hand, and against published values (Ralph et al. 2009). One-bond ^{1}H–^{13}C correlation (HSQC) spectra were acquired with an adiabatic Bruker pulse program hsqcetgpsisp2.2 and processed as described

previously (Kupče and Freeman 2007; Yelle et al. 2008). The semiquantitative HSQC NMR spectra were used to quantify arylglycerol-β-aryl ether units (A), resinols (C), syringyl units (S), and guaiacyl units (G) in the samples. The integration analysis for the α-proton (Hα) and α-carbon (Cα) of each structure was based on the methoxyl integral. This approach was taken because the lignin methoxyls are considered the most stable units in lignin, and demethylation or demethoxylation by pathogenic fungi is not expected because these reactions typically occur with saprophytic basidiomycetes. Although HSQC spectra are not strictly quantitative, the error in lignin structural determination is probably small because adiabatic pulse sequences were used to improve uniformity over the whole spectrum and to minimize effects due to coupling constant differences (Kupče and Freeman 2007). Moreover, the chemical environments of the Hα–Cα bond in lignin sidechains (A and C) are very similar to each other. We also determined the syringyl-to-guaiacyl (S:G) ratios. The S:G ratios are calculated by integrating the contours from the 2 or 2/6 positions of each type of aromatic unit. For example, the S integrals are logically divided by two because the 2 and 6 positions are identical in the symmetrical S units. All processing and integrations of the NMR spectra were performed with Bruker BioSpin's TopSpin 3.0 software for Mac. Klason lignin and carbohydrate analyses were performed at FPL (Madison, WI) on the samples via the NREL method (Sluiter 2008). A representative HSQC spectrum acquired on an almond wood control sample is provided in Supplementary Fig. S2. Statistical comparison of arylglycerol-β-aryl ether units (A), resinols (C), syringyl units (S), and guaiacyl units (G) in the pooled samples between treatments was performed via a paired *t* test in R version 3.6.

Biochemical composition of almond gum. The glycosyl composition of the gum was analyzed in a separate experiment. Plant material and inoculation method used were comparable to the ones used in susceptibility bioassays and wood chemistry analysis, with the exception that green stems (about 8 to 10 mm in diameter) were inoculated. Gum samples were collected 3 weeks after *N. parvum* inoculation, from three to five trees of each cultivar, with sterile spatulas. The collected gum samples were placed in plastic vials and stored at −20°C until analysis. Preparation of the gum for analysis was done by a modification of the alcohol-insoluble residue method of preparing plant cell walls for analysis (Fry 1988). Each gum sample (typically 0.5 to 1 g) was weighed, placed in liquid nitrogen in a mortar, and ground to a fine frozen powder with a pestle. The frozen powder was transferred with a small magnetic spin bar and aliquots of 95% (vol/vol) ethanol and water to achieve a suspension in 20 ml of 70% (vol/vol) ethanol in a 50-ml round bottom glass centrifuge tube with a Teflon-lined screw cap. The samples were stirred at 4°C for approximately 18 h to extract nonpolymeric components. The mixture was then applied to a nylon filtering cloth (Nitex, 15-µm pores) in a Buchner funnel on a vacuum filtering flask. The residue retained on the filtering cloth was rinsed six times with 10-ml aliquots of 70% ethanol and then three times with 10-ml aliquots of 100% acetone. The alcohol-insoluble residue of the gum was transferred by spatula from the nylon filtering cloth to glass vials. A single layer of Kimwipe was held with a rubber band over the opening of the vials, which were then placed in a simple vacuum desiccator overnight. The samples were then moved to a vacuum desiccator that contained phosphorus pentoxide (P_2O_5) desiccant for further drying (1 day) and storage until analysis (generally within 6 days).

Glass vials (4 ml) with Teflon-lined screw caps were used for performing glycosyl composition analysis as previously described (Fu et al. 2007), with some modifications. An internal standard of 100 nmol of inositol was first added to each vial as 10 µl of a 10-mM *myo*-inositol stock in water, which was then evaporated to dryness. Dry alcohol-insoluble gum residue (350 to 400 µg) was then weighed into each vial. For each day of glycosyl composition analysis, one additional vial containing sugar standards, each 100 nmol, was prepared by adding 100 µl of a stock mixture containing 1 mM of each of 10 authentic sugars, including *myo*-inositol, and evaporating that mixture to dryness. Subsequently, 400 µl of anhydrous 1.5 M HCl, 1.5 M methyl acetate in methanol was added to each vial, followed by an additional 100 µl of methyl acetate. The vials were then tightly closed with the Teflon-lined screw caps and placed in an 80°C dry heater block to incubate the methanolysis reaction overnight (14 to 18 h). The next morning, the vials were removed from the heater block and allowed to cool to room temperature. Five drops of t-butanol (to facilitate evaporation of HCl) were added to each vial, and the contents of the vials were then evaporated to dryness. A glass Pasteur pipet was used to quickly add five drops of the Tri-Sil HTP reagent to each vial. The Teflon-lined caps were quickly screwed on the vials, which were then manually tilted and rotated at room temperature for 15 min to steadily and thoroughly mix the contents of the vials to achieve complete trimethylsilylation of the sugars. After the 15-min reaction, the caps were removed from the vials, and the contents were evaporated to dryness. Iso-octane (200 µl) was added to each sample, one by one, before 1 µl was injected into the gas chromatograph (Hewlett Packard 5890 Series II gas chromatograph operating in the splitless mode of injection with a flame ionization detector). A fused silica capillary column (30 m length × 0.25 mm inside diameter × 0.25 µm film thickness; item number Rtx-1MS, Restek, Bellefonte, PA) was used with helium carrier gas flow of 0.63 ml/min (measured with oven held at 200°C). The injector and flame ionization detector temperatures were 250°C. The oven temperature program started at 105°C, held for 1 min, increased at 40°C per min to 160°C, held for 2 min, increased at 2°C per minute to 220°C, held for 0 min, increased at 40°C/min to 250°C, and held for 14 min before returning to 105°C. Integrated peak areas of the analyzed sugars were referenced to the peak area of the inositol internal standard in both the gum samples and the sugar standards when the abundance of sugar residues in the gum samples was calculated.

The glycosyl compositions of alcohol-insoluble residues of gums from different cultivars were compared in INSTAT software (version 2.0, GRAPHPAD Software, San Diego, CA) to generate a one-way ANOVA. The same software was used to perform the Tukey-Kramer pairwise comparison when ANOVA showed a significant effect of cultivars.

Histopathology of the almond–*N. parvum* interaction. Almond 'Nonpareil' was randomly selected for the histopathology study. Wood segments of the half trunk (i.e., 5 to 8 mm in radius and 40 mm in length) encompassing the point of inoculation and tissue above it were collected. Wood segments were placed immediately in 15-ml plastic tubes containing a formaldehyde, acetic acid, and ethyl alcohol (5:5:9) solution and kept for 48 h at 4°C, after which the solution was replaced by a solution of 80% ethyl-alcohol for storage at 4°C. Sections (70 µm thick) were obtained with a slicing microtome and a sapphire blade as described by Pouzoulet et al. (2017). Staining of specimen with toluidine O (0.05%, pH = 4.3, Sigma-Aldrich, St. Louis, MO), IKI (iodine potassium iodide; Ricca Chemical Company, Arlington, TX), and phloroglucinol/HCl (i.e., Wiesner reagent, Sigma-Aldrich) were performed via established protocols (Ruzin 1999). Light microscopy was done with a Leica DM 4000 upright microscope (Leica Microsystems CMS GmbH, Wetzlar, Germany).

For the covisualization of fungal hyphae by confocal microscopy, plant sections were placed in a 2-ml plastic tube containing 1 M potassium hydroxide and incubated 1 h in boiling water. Sections were then rinsed three times during 10 min in 100-mM phosphate buffer saline (PBS, pH 7) and incubated in 100 mM PBS containing 100 µg/ml of wheat germ agglutinin Alexa Fluor 488 conjugate (Life Technologies, Carlsbad, CA) for 2 h at 28°C before being rinsed one time with 100 mM PBS. Confocal micrographs were obtained with a Zeiss LSM 880 scanner (Zeiss, Oberkochen, Germany). Default manufacturer settings for Alexa Fluor 488 were used for the visualization of the fungal hyphae, and default manufacturer settings for the mCherry fluorescent protein were used for the visualization of plant structure (i.e., cell wall autofluorescence in the infrared band).

RESULTS

Evaluation of almond cultivars susceptibility to *N. parvum*. The four commercial almond cultivars 'Butte', 'Carmel', 'Monterey', and 'Nonpareil' were evaluated for their level of susceptibility to *N. parvum* after artificial inoculation. All the mock-inoculated plants developed a bark ridge that covered the inoculation wound (Fig. 1). Short reddish-brown discolorations were visible in inner woody tissue surrounding the wound. Gum exudates were visible on the inoculated wound 1 week after inoculation with *N. parvum*, whereas exudates were not observed in mock-inoculated plants. External signs of canker progression that include sunken dark lesions on the bark were also noticeable in *N. parvum*-inoculated plants. Dark, necrotic inner lesions that progressed toward the center of the trunk, and in lateral and longitudinal directions, were also observed. These necrotic lesions extended beyond the margin of the cankers in almost all plants (Fig. 2, Supplementary Fig. S3).

The relative susceptibility levels of the four almond cultivars toward *N. parvum* were determined by a measure of the longitudinal length of the cankers and the inner necrotic lesions (Fig. 2, Table 1). Weak, positive correlation was found between necrotic lesion length and canker length (Supplementary Figs. S1 and S3). Treatment type (mock vs. *N. parvum* inoculation) was the only parameter with a significant effect on the length of the necrotic lesion that developed in the xylem ($P < 0.001$). Differences in canker length were found between cultivars ($P < 0.001$) but were not replicated in the second experiment ($P = 0.09$). Pairwise comparisons confirmed the classification of cultivars in three different statistical classes for this second experiment, with 'Butte' manifesting significantly longer cankers than 'Carmel' and 'Monterey'. Overall, comparison of both canker and internal necrotic lesion lengths did not show a consistent difference in almond cultivar susceptibility to *N. parvum*.

Biochemical composition of almond wood cell walls after *N. parvum* infection. The wood samples were subjected to chemical composition analysis to determine the quantities of lignin and structural carbohydrates present in almond cell walls and how those quantities were affected by *N. parvum* colonization (Fig. 3A). Our method yielded 75.3% ± 2.6% and 76.9% ± 2.5% of the total dry weight for mock controls and *N. parvum*-inoculated samples, respectively. Using pooled data from the four cultivars, we observed a significant loss of structural glucose ($P < 0.05$) and a significant increase of lignin and arabinose ($P < 0.01$) in *N. parvum*-inoculated compared with the mock-inoculated trees, whereas xylose, galactose, and mannose also increased but were not statistically significant. However, of the four cultivars, only 'Nonpareil' did not show a reduction in glucose and only a slight increase in lignin (Supplementary Table S1), and these observations were consistent in each replicate. In contrast, the almond cultivar 'Carmel' displayed the highest reduction in xylose and, along with 'Monterey', the highest percentage increase in lignin.

The 2D HSQC integration data indicated that *N. parvum*-inoculated almond wood displayed a higher number of lignin interunit linkages than the mock-inoculated wood (Table 2, Supplementary Table S2). The syringyl/guaiacyl (S/G) unit ratios tended to decrease when the mock-inoculated pools were compared with the *N. parvum*-inoculated versions for all four almond cultivars ($P = 0.057$), and this decrease was the most pronounced for 'Nonpareil'. The change in S/G unit ratios was driven mostly by a higher guaiacyl unit content, although this trend was not statistically significant ($P = 0.066$).

Biochemical composition of almond gum. The glycosyl compositions of gums showed statistically significant differences between cultivars occurring for rhamnosyl, glucuronosyl, and 4-*O*-methylglucuronosyl residues (Supplementary Table S3). Overall, the most abundant (by percentage mole) glycosyl residues found in these almond gums were arabinosyl (35.2 ± 2.7%), galactosyl (30.4 ± 1.6%), xylosyl (16.4 ± 2.8%), glucuronosyl (6.9 ± 1%), mannosyl (3.7 ± 0.2%), 4-*O*-methylglucuronsyl (3.2 ± 1.3%), and rhamnosyl (2.9 ± 0.5%) (Fig. 3B). The glucosyl, fucosyl, and galacturonosyl residues taken together represented <2% of the total glycosyl residues of these gums.

Histopathology of the almond–*N. parvum* interaction. Almond response to *N. parvum* infection was further characterized at the histological level with the commercial standard 'Nonpareil'. The first noticeable phenotype of *N. parvum* infection compared with mock controls was the decay of the bark around the inoculation wound and the presence of continuous ring of gum ducts within newly formed secondary xylem tissue (Fig. 4). Gum ducts were either absent or rare in cross-sections of mock-inoculated plants (Fig. 4A). Gum ducts were located within fascicular portions and were separated by apparently intact rays (Fig. 4B and Fig. 5A and B). Within the xylem before the wound, a depletion of starch was

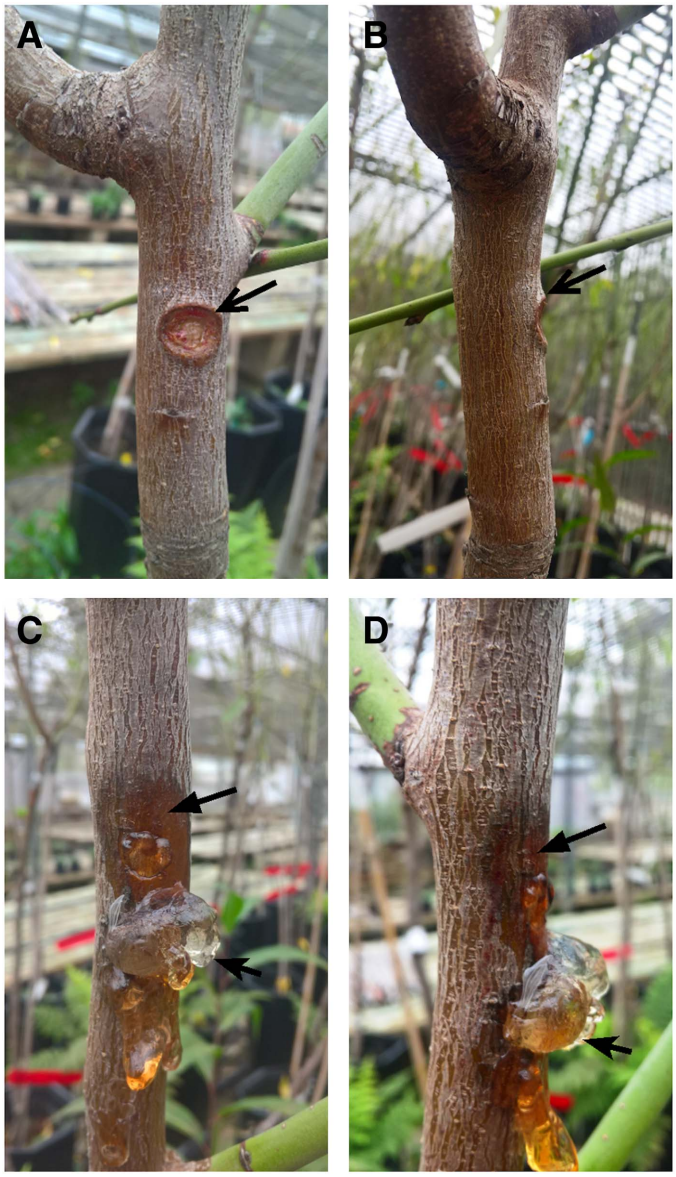

Fig. 1. External symptoms of *Neofusicoccum parvum* infection observed in experimental trials 6 weeks after inoculation. **A and B,** Phenotype of wounded, mock-inoculated plant. Note the formation of the bark ridge around the wound and the absence of gum exudates (open-head arrows). **C and D,** Phenotype of *N. parvum*-inoculated plant. Note the development of canker, characterized by the darkening of the bark and the formation of depression underneath it around the inoculation wound (solid-head arrows). Note the heavy production of gum exudates coming out of the wound (notched-head arrows).

noticeable in both the mock- and *N. parvum*-inoculated plants. This depletion extended further radially and beyond the margin of the inoculation wound in *N. parvum*-inoculated plants (Fig. 4A and B). Phloroglucinol/HCl (Wiesner's reagent) staining showed that a complete lack of lignin (Blaschek et al. 2020) occurred within parenchyma surrounding the gum ducts (Fig. 4D). An increase in the stain intensity with the Wiesner reagent indicated that within the xylem area surrounding the wounds, local accumulation of guaiacyl lignin units occurred in both the mock- and *N. parvum*-inoculated plants. Similar to the depletion of starch, the areas where the accumulation of lignin could be noticed in *N. parvum*-inoculated plants were not restricted to the first to second millimeter of xylem below the surface of the wound, as opposed to the mock-inoculated controls (Fig. 4C and D). Observations at higher magnification revealed that these lignin depositions occurred as discrete dots in the walls of vessels and axial parenchyma cells (Fig. 5C and D). The lignification of the tyloses walls could also be observed in occluded vessels (Fig. 5C and D).

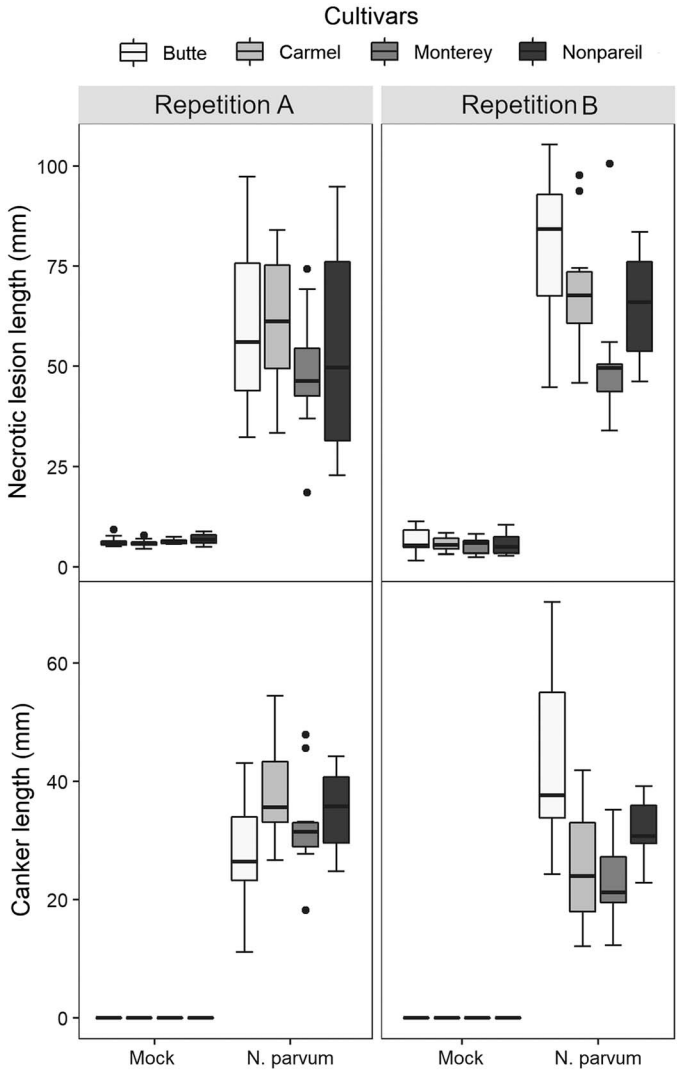

Fig. 2. Susceptibility of four *Prunus dulcis* L. cultivars to *Neofusicoccum parvum* inoculation. Results from two different trials are displayed (i.e., repetitions A and B). Susceptibility was evaluated through the longitudinal length of inner necrotic lesions (upper plots) and cankers (lower plots). Note that cankers were not observed in mock-inoculated controls. $n = 10$ for each cultivar and treatment in both replicates. Bottom and top of the boxes represent 25th and 75th percentiles of the data, respectively, and the centerline represents the median. Minimum and maximum whiskers represent the smallest and largest values, respectively, within 1.5 times the interquartile range below and above the 25th and 75th percentiles. Outliers, when present, are represented by dots.

Tracking of fungal hyphae in almond wood with wheat germ agglutinin-Alexa Fluor conjugate revealed that *N. parvum* effectively colonized the xylem of its host, although it did not degrade the structure of the cell walls extensively. Careful observation of the mock-inoculated control samples confirm that no fungal hyphae could be observed in the xylem tissue near the inoculation wound (Fig. 6A), whereas with the *N. parvum*-inoculated plants, numerous structures of hyphae were easily identified in cross-section (Fig. 6B). Overall, hyphae structures were located within the lumen of xylem vessels and within the lumen of xylem parenchyma including rays (Fig. 6C, D, and E). Neither cell wall degradation nor hyphae structure located within the cell wall was detected among the samples observed. Observation of plant tissue sections above the inoculation wounds revealed that dense networks of hyphae could be present within the lumen of xylem vessels (Fig. 6C, D, and E). It also revealed that the gum duct might not present an impervious barrier toward the spread of this pathogen, because hyphae could be observed from either of its margins (Fig. 6E).

DISCUSSION

Our results overall suggested that there was no difference in the level of resistance of the four almond cultivars to *N. parvum*. 'Butte' developed significantly larger cankers than 'Carmel' and 'Monterey' in one repetition of our bioassay, but the length of necrotic lesions and the second experiment did not support these results. This inconsistency, and the absence of clear differences in the level of resistance of cultivars, is in line with previous observations (Olmo et al. 2016) but also conflicts with other studies on almond and other *Prunus* species (English et al. 1975; Mancero-Castillo et al. 2018). The number of cultivars used in our study was low, and larger screening of plant genetic materials or longer incubation periods would help segregate genotype susceptibility to wood canker pathogens. English et al. (1975) reported contrasting levels of resistance across three almond cultivars to *B. dothidea* after experimental inoculation and ranked them from most susceptible ('Nonpareil') to least susceptible ('Mission'). Surveys in several almond production areas globally revealed that various Botryosphaeriaceae species caused wood cankers (Holland et al. 2021; Inderbitzin et al. 2010; Olmo et al. 2016; Sohrabi et al. 2020). These studies also stressed that *B. dothidea* might not be the most aggressive and prevalent pathogen among those causing canker diseases in almond (Holland et al. 2021; Inderbitzin et al. 2010). Perhaps *B. dothidea* used by English et al. (1975) was a different taxon (Inderbitzin et al. 2010), given that the nomenclature of this family has recently been revised (Dissanayake et al. 2016; Slippers et al. 2004). Interestingly, *P. dulcis* 'Tardy-Nonpareil', a 'Nonpareil' bud-sport, has been proposed as a genetic source of resistance to peach gummosis, a disease caused by *B. dothidea* in *Prunus persica* in the southeastern United States (Mancero-Castillo et al. 2018). In this context, it would be interesting to test whether 'Tardy-Nonpareil' behaves differently from its apparently vulnerable parent 'Nonpareil' and whether this resistance stands against a larger variety of taxa in the Botryosphaeriaceae with contrasted aggressiveness like *N. parvum*.

Virulent pathogens are particularly detrimental to host longevity because of their ability to kill the vascular cambium, which is characterized by the formation of cankers underneath the bark. Here we found that on a plant-to-plant basis, the lengths of necrosis in the xylem significantly exceeded canker lengths. This finding suggests that the longitudinal colonization of tissue by *N. parvum* is achieved faster in the xylem than in the bark and that the outward movement of the pathogen, from the infected xylem column toward the vascular cambium, is hindered. Dense networks of hyphae were found in open vessels, which confirmed that a fast and intensive colonization of conduits is achieved. This quick invasion of host vasculature probably precedes further colonization of surrounding xylem tissue.

Gum ducts were found to develop in locations where the latest growth ring of xylem formed, underneath the vascular cambium.

Xylem response to wounding or biotic infection of most perennials is accompanied by the edification of a so-called barrier zone (i.e., compartmentalization of decay in trees [CODIT] wall 4) (Morris et al. 2020; Shigo 1984). This barrier zone is produced by the vascular cambium after injury and consists of reinforced xylem tissue that is aimed at protecting the cambium from biotic threats. Thus, the barrier retains the ability of the tree to produce functional secondary xylem upon infection and is pivotal in promoting perennial host survival (Morris et al. 2020; Pearce 1996). We hypothesize that gum ducts in *Prunus* species serve a similar function to the barrier zone in other woody species, even if they do not derive from a common histological origin because gum ducts are schizogenous structures (Biggs and Britton 1988; Bouaziz et al. 2016b). From a mechanistic standpoint, it can be easily understood how cell wall reinforcement and accumulation of antifungal compounds observed within barrier zones can impede the pathogen's progression (Morris et al. 2020). The meaning behind the gum duct layer within CODIT nonetheless appears unclear. By developing gum or resin ducts, the host is creating an extended chemical boundary, which might block pathogen invasion. Direct evidence of antibacterial properties was found for some bioactive polyphenols and volatile compounds of almond gum (Bouaziz et al. 2017), but antifungal properties have yet to be demonstrated. One drawback of gum duct formation is that the host is also creating equal amounts of structural void that can potentially be crossed easily by an aggressive fungus such as *N. parvum*. Hence, fungal hyphae were detected within and near to the gum ducts, indicating that this response from the plant host might not provide an impervious barrier to *N. parvum* spread, even if the colonization achieved in these ducts seemed far less severe than the one observed in neighboring vessels. Secretory ducts appeared early on in vascular plants' history, probably as a defense mechanism against insects and microbial pathogens. There is evidence of loss and reappearance of resin ducts and laticifers along plant evolution and across many gymnosperm and angiosperm taxa, underlying the critical role of such secretory structures in plants species adaptation to their habitats (Prado and Demarco 2018).

In *Prunus* species, gummosis is a common reaction to infection by fungal canker pathogens (Bouaziz et al. 2016b; Ezra et al. 2017; Holland et al. 2021; Li et al. 2014) and was reported to be triggered by a variety of abiotic and biotic factors, such as drought, wounding, and insect and microbial attacks (Bouaziz et al. 2016b). We never observed exudation of gum or formation of gum ducts after pruning of the mock-inoculated trees. In this context, one can suggest that gummosis is a specific response triggered by biotic aggression in almond under our conditions. Previous works provided evidence that gummosis and the formation of traumatic ducts can be triggered by phytohormones (i.e., ethylene, methyl jasmonate, ethephon) in both angiosperms and gymnosperms (Hudgins and Franceschi 2004; Morrison et al. 1987; Olien and Bukovac 1982; Saniewski et al. 1998, 2006). Ethylene and jasmonic acid are key phytohormones known to act along the signaling pathway, operating in response to infection by necrotrophic pathogens such as *N. parvum* (Bürger and Chory 2019). However, these hormones also mediate plant response to only wounding with no pathogen invasion (Vega-Muñoz et al. 2020). Gum ducts are schizogenous spaces surrounded by secretory cells and then derive from preexisting xylem parenchyma (Bouaziz et al. 2016b). This involves important developmental and metabolic processes so that the cell wall middle lamella breaks down and biosynthesis of gum polymers can be achieved by secretory cells surrounding the remaining channel (Gao et al. 2016). Recent studies from Zhang et al. (2019) provided evidence of hormonal feedback that would prevent plants from overreacting to wounding. Although wounding may have the potential to induce gum duct development through the action of ethylene and jasmonic acid, it is possible that the conditions of concentration and the time during which tissue must be exposed to these hormones to initiate the development of gum ducts were not met in our experimental conditions. It is also possible that the development of gummosis attributed to wounding in other studies may have resulted from unwanted biotic infection that remained unnoticed.

The role of almond gum in the interaction with fungal canker pathogens remains hypothetical, but because of its chemical properties it has been used as an emulsifier (Bouaziz et al. 2017; Mahfoudhi et al. 2014) and for other applications in the food industry (Bouaziz et al. 2016a, 2017). The glycosyl composition of almond gum was similar to that of arabinogalactan proteins. In particular, the arabinosyl and galactosyl contents were high, with appreciable amounts of glucuronosyl, 4-*O*-methylglucuronosyl, and rhamnosyl residues also present. These glycosyl residues are characteristic of arabinogalactan proteins from many plant species (Serpe and Nothnagel 1999). Arabinogalactan proteins from some plants contain small amounts of xylosyl residues, but higher xylosyl contents in the

TABLE 1. Analysis by variance output from the susceptibility bioassays of four *Prunus dulcis* L. cultivars to *Neofusicoccum parvum* inoculation[a]

Response variable	Repetition	Sources of variation	SS	Degrees of freedom	F	*P*
Necrotic lesion length	A	Cultivar	0.02	3	0.29	0.83
		Block	0.01	1	0.01	0.97
		Treatment	16.86	1	857.98	<0.001***
		Cultivar × block	0.02	3	0.34	0.79
		Cultivar × treatment	0.08	3	1.32	0.28
		Block × treatment	0.01	1	0.62	0.44
		Cultivar × block × treatment	0.01	3	0.17	0.92
	B	Cultivar	0.18	3	2.39	0.08
		Block	0.02	1	0.88	0.35
		Treatment	23.21	1	934.54	<0.001***
		Cultivar × block	0.04	3	0.48	0.69
		Cultivar × treatment	0.04	3	0.59	0.62
		Block × treatment	0.07	1	2.75	0.10
		Cultivar × block × treatment	0.15	3	2.01	0.12
Canker length	A	Cultivar	527.9	3	2.36	0.09
		Block	29.52	1	0.39	0.53
		Cultivar × block	170.73	3	0.76	0.52
	B	Cultivar	2457.7	3	7.35	<0.001***
		Block	0.20	1	0.01	0.96
		Cultivar × block	10.20	3	0.03	0.99

[a] Cankers were not observed in mock-inoculated controls, and thus the effect of inoculation was not tested in this analysis. $n = 10$ plants per cultivar and treatment in each replicate. Each replicate was split in two blocks on two separate benches. The blocks were randomly distributed on the bench and consisted of five plants of each cultivar and treatment. SS is the sum of squares; F is the F-statistics; *P* is the *P* value associated with the F-test.

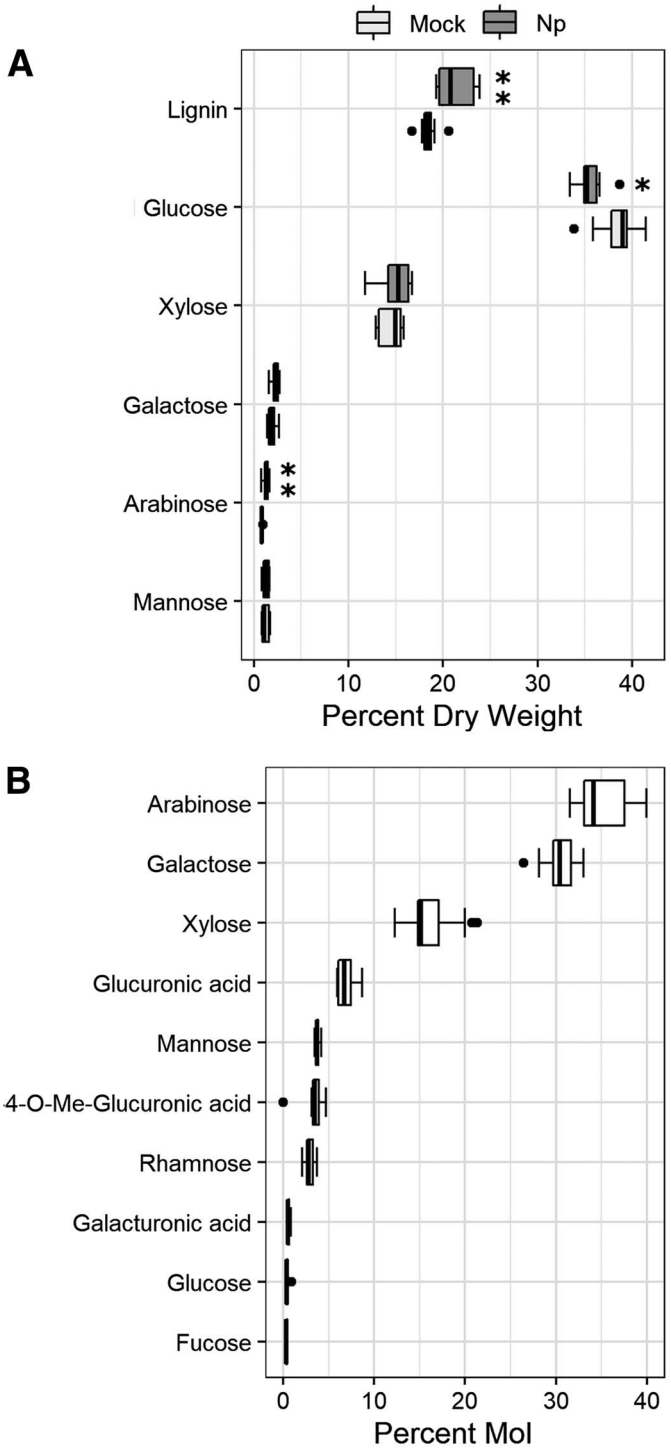

Fig. 3. Major structural components of almond wood cell wall and gum. **A,** Percentage dry weight data for almond wood cell wall composition for mock- and *Neofusicoccum parvum*-inoculated plants. These data encompass the pooled samples from four cultivars 'Carmel', 'Butte', 'Nonpareil', and 'Monterey' for 2 years (n = 8). *Value significantly different (P < 0.05); **value significantly different (P < 0.01). **B,** Glycosyl composition (mole percent) of almond tree/plant gum from *N. parvum*-inoculated plants. These data encompass the four cultivars 'Carmel', 'Butte', 'Nonpareil', and 'Monterey' for 2 years (n = 8). Bottom and top of the boxes represent 25th and 75th percentiles of the data, respectively, and the centerline represents the median. Minimum and maximum whiskers represent respectively the smallest and largest values within 1.5 times the interquartile range below and above the 25th and 75th percentiles. Outliers, when present, are represented by dots.

range of 14 to 17 mole percent, as found in these almond gums, usually do not occur in arabinogalactan proteins. Thus, it seems likely that some amount of xylosyl containing polymer, perhaps a hemicellulose, was also present in the gums. The presence of arabinogalactan proteins and hemicellulose in almond gum has been previously reported by Bouaziz et al. (2016b), although in that study hemicellulose was the dominant component in gums from trees of unknown pathogen status. The galacturonosyl contents were very low in all gums in the present study, indicating that little or no pectic polysaccharides were present in the gum. The glucosyl contents were also very low in all of the gums, indicating the presence of little or no noncellulosic glucan such as callose or xyloglucan hemicellulose. Attributing these divergences of gum chemistry to the specificity of the host–pathogen interaction would be speculative at this stage. Nonetheless, it would be interesting to test whether different biotic interactions induce changes in chemical composition of the gum.

Overall, *N. parvum* infection induced structural and chemical changes of the xylem of almond trees. These changes can

TABLE 2. Two-dimensional nuclear magnetic resonance integral data for lignin interunit linkages relative to the lignin methoxyl and aromatic unit ratios in cell walls of almond wood for mock-inoculated plants and plants inoculated with the pathogenic fungus *Neofusicoccum parvum*[a]

Treatment	Arylglycerol β-aryl ether (β-O-4) linkage	Resinol (β-β) linkage	Syringyl/ guaiacyl ratio
Mock-inoculated	0.062 ± 0.034	0.015 ± 0.0041	4.54 ± 1.18
N. parvum-inoculated	0.066 ± 0.04	0.018 ± 0.0021	3.79 ± 0.76

[a] Data encompass the pooled samples from four cultivars: 'Carmel', 'Butte', 'Nonpareil', and 'Monterey' for 2 years (n = 8).

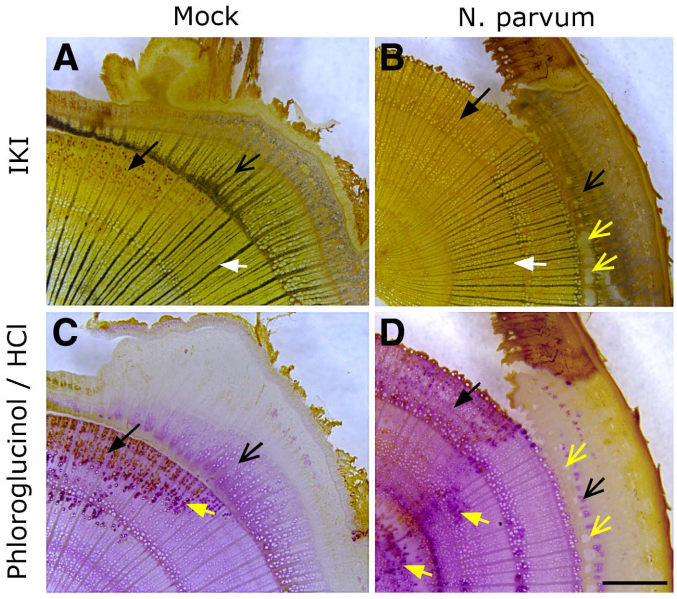

Fig. 4. Micrographs of trunk cross-section within the inoculation wound in mock- and *Neofusicoccum parvum*-inoculated *Prunus dulcis* L. trees 'Nonpareil'. **A,** Mock- and **B,** *N. parvum*-inoculated samples stained with iodine-potassium-iodine (IKI), a histological test for starch presence (i.e., stain in deep black; see white solid-head arrows). **C,** Mock- and **D,** *N. parvum*-inoculated samples stained with phloroglucinol/HCl (i.e., Wiesner reagent), a histological test for guaiacyl lignin units (i.e., stained in purple). Black solid-head arrows indicate area of the xylem existing before the wound and in the vicinity of the latter. Black open-head arrows indicate secondary xylem formed after the wounding. Yellow open-head arrows indicate the presence of gum ducts in **B** and **D**. Yellow solid-head arrows indicate the presence of guaiacyl-ich areas in **C** and **D**. All micrographs are displayed at the same magnification. Scale bar = 1,000 µm.

be interpreted as the results of the host response to infection with gum duct development and the action of pathogen on cell wall structure and chemical composition. Glycosyl composition of gums was generally consistent with minor differences observed across almond cultivars analyzed. Because the major components of gums (arabinose, galactose and xylose) were recovered in higher proportion in wood from *N. parvum*-inoculated than mock-inoculated samples, one can assume that changes in the carbohydrates were the result of the presence of gum residuals in the wood samples or occurred because the decrease in glucose resulted in a proportional increase of the other sugars. These data coupled with our histological study suggest that *N. parvum* may not be able to break down the carbohydrate backbone of almond gum in order to metabolize its monosaccharide-forming units but rather preferentially targets glucose monomers and polymers. Our analytic method essentially measured structural carbohydrates (Sluiter 2008) and thus the significant depletion of glucose probably originates from the breakdown of major cell wall polysaccharides (i.e., xyloglucan and cellulose) as previously shown in other pathosystems (Rolshausen et al. 2008). Evidence of cell wall colonization by *N. parvum* could not be clearly established by histological means in our current study, but previous reports provided evidence that this pathogen possess the genetic makeup and enzymatic arsenal to do so (Massonnet et al. 2018; Morales-Cruz et al. 2015). However, our data also suggested a depletion of nonstructural carbohydrate stored into the xylem (i.e., starch), indicating that perhaps *N. parvum* preferentially targets glucose stored as starch over structural glucose in cell walls because it is a less metabolically taxing strategy. This may explain the low decrease in structural glucose observed for some almond cultivars such as 'Nonpareil' that may have a higher starch content stored in parenchyma cells. Decrease in starch in the xylem tissues of woody hosts was commonly observed as a response to infection by bacterial and fungal vascular pathogens (Ingel et al. 2021; Pouzoulet et al. 2017; Rolshausen et al. 2008). This plant energy reserve could play a pivotal role and become metabolized by either the host to wall off the wound against potential invaders or the pathogen for pathogenesis.

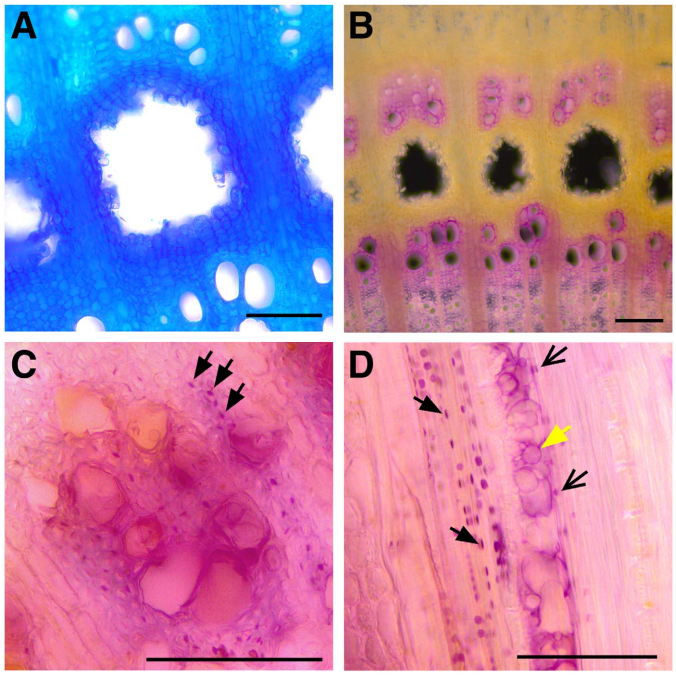

Fig. 5. Histological responses observed in the trunk of wounded and *Neofusicoccum parvum*-inoculated *Prunus dulcis* L. trees 'Nonpareil'. **A,** Cross-section of a gum duct that developed in *N. parvum*-inoculated plants (stained with toluidine blue O). **B,** Gum ducts that developed in *N. parvum*-inoculated plants (stained with phloroglucinol/HCl as a test for guaiacyl lignin units, i.e., purple stain). Note the absence of stain showing a complete depletion of guaiacyl lignin in the wall of cells surrounding the gum ducts. **C,** Close-up view of cross-section of xylem area where guaiacyl accumulation is observed in response to *N. parvum* infection (stained with phloroglucinol/HCl). **D,** Micrographs of a longitudinal section (stained with phloroglucinol/HCl) in a xylem area similar to **C**. Note the localization of the purple stain showing that the accumulation of guaiacyl lignin units occurred in discrete spots in xylem parenchyma cells (black solid-head arrows in **C** and **D**), in vessel walls (black open-head arrows in **D**), and in the wall of tyloses in vessels (yellow solid-head arrow in **D**). Scale bar = 100 µm.

The xylem response to infection was marked by a significant increase in lignin, indicating a cell wall reinforcement to wall off *N. parvum*. One might expect the syringyl content be higher in the pathogen-inoculated plants, because syringyl units are more dominant in hardwood species (Ralph et al. 2019). However, the trend we observed suggests that the host puts more emphasis on strengthening walls with guaiacyl over syringyl units in response to *N. parvum* colonization, as shown by using the Wiesner reagent (Blaschek et al. 2020). The global enrichment in guaiacyl, as perceived in cross-sections because of the apparent staining of the whole wall, should be considered with caution and may result from the diffraction of light within the 70-µm-thick xylem slices in the cell walls from numerous small elements that are strongly stained. The discrete nature of the guaiacyl-rich deposits observed in longitudinal section suggested that strategic reinforcements operated at the level of the cell wall, probably to seal off pits and plasmodesmata spanning through the walls. Although there was not an obvious sign of alteration of the cell wall within infected tissues, the presence and the spread of the fungus were noticed within the lumen of the cell of the xylem parenchyma, which implies that the fungus spread from cell to cell and thus crossed the wall. English et al. (1975) and Biggs and Britton (1988) reported the ability of Botryosphaeriaceae to cross the cell wall of *Prunus* host through pits. In this context, sealing off pit pairs might slow down the progression of the fungus within parenchyma, although this action does not fully impede its movement. Sealing of intercellular channels such as plasmodesmata is characterized by deposition of callose (Wu et al. 2018). Our observations provide clues about the potential role of lignin in such processes in the xylem of perennial hosts. A guaiacyl-rich material was also detected within the wall of the tyloses occluding the xylem vessels. Such lignified layers were observed in the tylose wall of other perennials (De Micco et al. 2016) and probably participated to some extent in the chemical changes observed with *N. parvum* infection.

In conclusion, the molecular, biochemical, and histological approach of interaction between the almond tree and the canker fungal pathogen *N. parvum* suggested that there was not a clear difference in susceptibility across commercial cultivars widely used in California orchards. Gummosis (exudation of gums) was triggered by pathogenic infection but not by wounding, and the host response to infection was characterized by biochemical changes in the glycosyl and lignin fractions that can be attributed to both the formation of gum ducts and xylem cell wall modifications. These responses seemed to occur in a strategic fashion to reinforce wall 4 and protect the tree cambium and may delay the progression of the *N. parvum* into the trunk. However, our results confirmed the high vulnerability of almond toward this cosmopolitan and aggressive plant pathogen.

ACKNOWLEDGMENTS

We thank undergraduate students Jiha Lee and Allison Cid for their participation in the work on almond gum, Raphael Reyes for help with infections, Vanessa Escolero for help with potting, and Fred Matt (USDA FPL) for performing the Klason lignin and carbohydrate analyses of the almond wood.

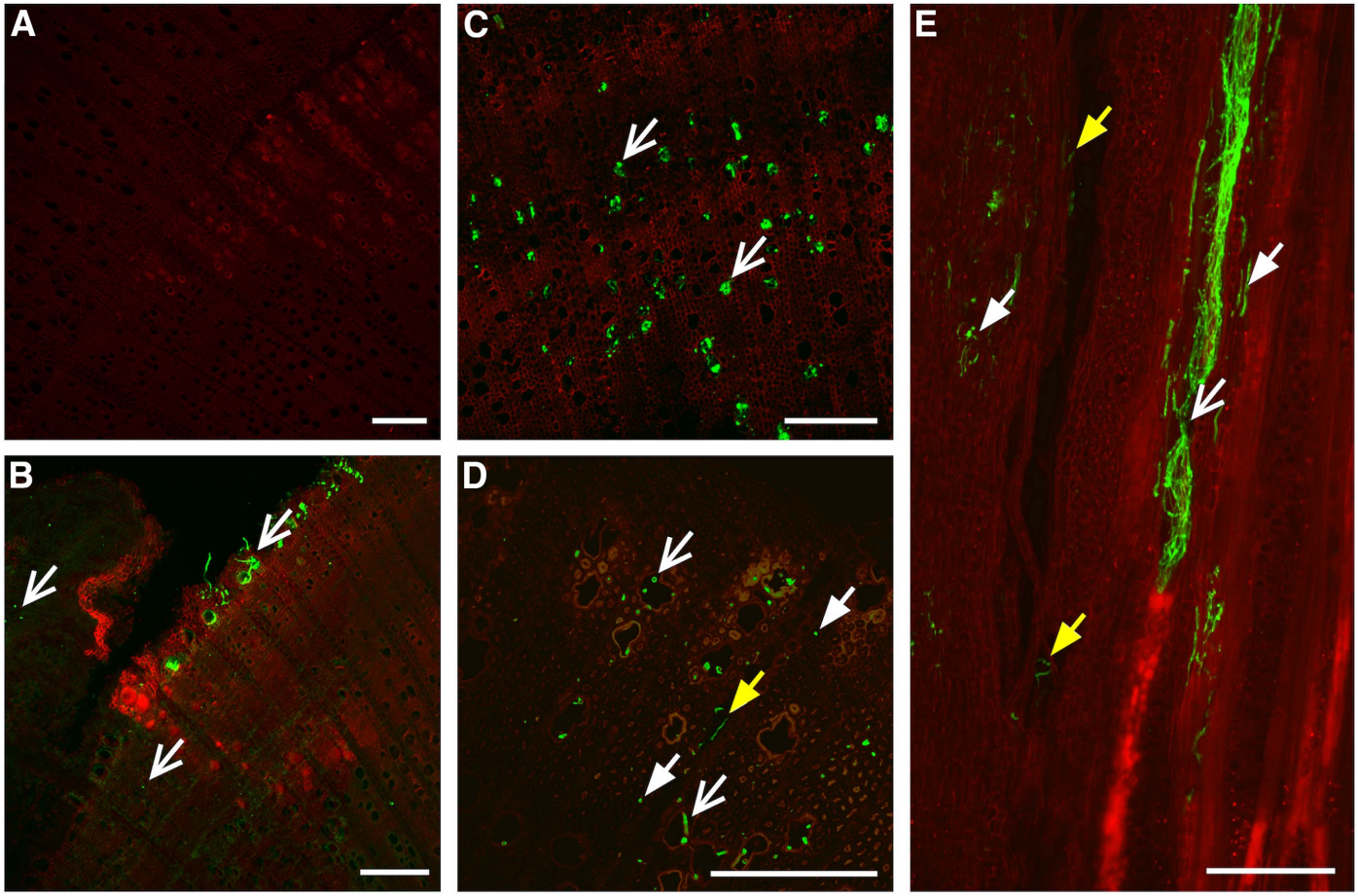

Fig. 6. In situ visualization of fungal structures in wounded and *N. parvum*-inoculated *Prunus dulcis* L. 'Nonpareil' trees. Fungal cell wall is labeled with a wheat germ agglutinin (WGA)–Alexa Fluor conjugate probe, and micrographs were obtained with a confocal fluorescence microscope. Specific probe signal (green) and autofluorescence plant signal (red) are overlaid. **A,** Micrograph of mock-inoculated trunk at the margin of the inoculation wound (i.e., the area displayed is similar to the one displayed in Fig. 4A). No signal associated with the WGA–Alexa Fluor conjugate (green) is observed. **B,** Micrograph of *N. parvum*-inoculated plant at the margin of the wound (i.e., the area displayed is similar to the one displayed in Fig. 4B). Fungus (green) can be seen at the surface of the wound but also within xylem tissue more distal from the inoculation wound (open-head arrows). **C,** A cross-section of a necrotic lesion in *N. parvum*-inoculated plant showing fungal structures located mostly in xylem vessels (open-head arrows). **D,** Close-up view of necrotic lesion in the trunk of a *N. parvum*-inoculated plant showing fungal structures in xylem vessels (white open-head arrows), axial parenchyma cells (white solid-head arrows), and ray parenchyma cells (yellow solid-head arrow). **E,** Longitudinal section of necrotic lesion of *N. parvum*-inoculated plant showing the presence of a dense network of fungal hyphae in xylem vessels (white open-head arrow), axial parenchyma cells (white solid-head arrows), and gum duct (yellow solid-head arrows). Note the heavy colonization achieved in the vessel (left) compared with the one observed in the gum duct (right). Also note that the fungal structures are present from either side of the gum duct. Scale bar = 200 µm.

LITERATURE CITED

Adesemoye, A. O., Mayorquin, J. S., Wang, D. H., Twizeyimana, M., Lynch, S. C., and Eskalen, A. 2014. Identification of species of Botryosphaeriaceae causing Bot gummosis in citrus in California. Plant Dis. 98:55-61.

Agustí-Brisach, C., Moldero, D., Raya, M. del C., Lorite, I. J., Orgaz, F., and Trapero, A. 2020. Water stress enhances the progression of branch dieback and almond decline under field conditions. Plants 9:1213.

Batista, E., Lopes, A., and Alves, A. 2021. What do we know about Botryosphaeriaceae? An overview of a worldwide cured dataset. Forests 12:313.

Biggs, A. R., and Britton, K. O. 1988. Presymptom histopathology of peach trees inoculated with *Botryosphaeria obtusa* and *B. dothidea.* Phytopathology 78:1109-1118.

Blaschek, L., Champagne, A., Dimotakis, C., Nuoendagula, Decou, R., Hishiyama, S., Kratzer, S., Kajita, S., and Pesquet, E. 2020. Cellular and genetic regulation of conifer aldehyde incorporation in lignin of herbaceous and woody plants by quantitative Wiesner staining. Front. Plant Sci. 11:109.

Bouaziz, F., Koubaa, M., Ben Jeddou, K., Kallel, F., Boisset Helbert, C., Khelfa, A., Ghorbel, R. E., and Chaabouni, S. E. 2016a. Water-soluble polysaccharides and hemicelluloses from almond gum: Functional and prebiotic properties. Int. J. Biol. Macromol. 93:359-368.

Bouaziz, F., Koubaa, M., Chaabene, M., Barba, F. J., Ghorbel, R. E., and Chaabouni, S. E. 2017. High throughput screening for bioactive volatile compounds and polyphenols from almond (*Prunus amygdalus*) gum: Assessment of their antioxidant and antibacterial activities. J. Food Process. Preserv. 41:e12996.

Bouaziz, F., Koubaa, M., Ellouz Ghorbel, R., and Ellouz Chaabouni, S. 2016b. Recent advances in Rosaceae gum exudates: From synthesis to food and non-food applications. Int. J. Biol. Macromol. 86:535-545.

Bürger, M., and Chory, J. 2019. Stressed out about hormones: How plants orchestrate immunity. Cell Host Microbe 26:163-172.

Cantu, D., Vicente, A. R., Labavitch, J. M., Bennett, A. B., and Powell, A. L. T. 2008. Strangers in the matrix: Plant cell walls and pathogen susceptibility. Trends Plant Sci. 13:610-617.

De Micco, V. D., Balzano, A., Wheeler, E. A., and Baas, P. 2016. Tyloses and gums: A review of structure, function and occurrence of vessel occlusions. IAWA J. 37:186-205.

Dissanayake, A. J., Phillips, A. J. L., Li, X. H., and Hyde, K. D. 2016. Botryosphaeriaceae: Current status of genera and species. Mycosp. 7:1001-1073.

English, H., Davis, J. R., and DeVay, J. E. 1975. Relationship of *Botryosphaeria dothidae* and *Hendersonula toruloidea* to a canker disease of almond. Phytopathology 65:114-122.

Ezra, D., Hershcovich, M., and Shtienberg, D. 2017. Insights into the etiology of gummosis syndrome of deciduous fruit trees in Israel and its impact on tree productivity. Plant Dis. 101:1354-1361.

Fry, S. C. 1988. The Growing Plant Cell Wall: Chemical and Metabolic Analysis. Longman Group Limited, London.

Fu, H., Yadav, M. P., and Nothnagel, E. A. 2007. *Physcomitrella* patens arabinogalactan proteins contain abundant terminal 3-O-methyl-l-rhamnosyl residues not found in angiosperms. Planta 226:1511-1524.

Gao, L., Wang, Y., Li, Z., Zhang, H., Ye, J., and Li, G. 2016. Gene expression changes during the gummosis development of peach shoots in response to *Lasiodiplodia theobromae* infection using RNA-seq. Front. Physiol. 7:170.

Gramaje, D., Baumgartner, K., Halleen, F., Mostert, L., Sosnowski, M. R., Úrbez-Torres, J. R., and Armengol, J. 2016. Fungal trunk diseases: A problem beyond grapevines? Plant Pathol. 65:355-356.

Holland, L. A., Trouillas, F. P., Nouri, M. T., Lawrence, D. P., Crespo, M., Doll, D. A., Duncan, R. A., Holtz, B. A., Culumber, C. M., Yaghmour, M. A., Niederholzer, F. J. A., Lightle, D. M., Jarvis-Shean, K. S., Gordon, P. E., and Fichtner, E. J. 2021. Fungal pathogens associated with canker diseases of almond in California. Plant Dis. 105:346-360.

Hudgins, J. W., and Franceschi, V. R. 2004. Methyl jasmonate-induced ethylene production is responsible for conifer phloem defense responses and reprogramming of stem cambial zone for traumatic resin duct formation. Plant Physiol. 135:2134-2149.

Inderbitzin, P., Bostock, R. M., Trouillas, F. P., and Michailides, T. J. 2010. A six locus phylogeny reveals high species diversity in Botryosphaeriaceae from California almond. Mycologia 102:1350-1368.

Ingel, B., Reyes, C., Massonnet, M., Boudreau, B., Sun, Y., Sun, Q., McElrone, A. J., Cantu, D., and Roper, M. C. 2021. *Xylella fastidiosa* causes transcriptional shifts that precede tylose formation and starch depletion in xylem. Mol. Plant Pathol. 22:175-188.

Kupče, E., and Freeman, R. 2007. Compensated adiabatic inversion pulses: Broadband INEPT and HSQC. J. Magn. Reson. 187:258-265.

Li, Z., Wang, Y.-T., Gao, L., Wang, F., Ye, J.-L., and Li, G.-H. 2014. Biochemical changes and defence responses during the development of peach gummosis caused by *Lasiodiplodia theobromae.* Eur. J. Plant Pathol. 138: 195-207.

López-Moral, A., Lovera, M., Raya, M. del C., Cortés-Cosano, N., Arquero, O., Trapero, A., and Brisach, C. A. 2020. Etiology of branch dieback and shoot blight of English walnut caused by Botryosphaeriaceae and Diaporthe species in southern Spain. Plant Dis. 104:533-550.

Lu, F., and Ralph, J. 2003. Non-degradative dissolution and acetylation of ball-milled plant cell walls: High-resolution solution-state NMR. Plant J. 35:535-544.

Mahfoudhi, N., Sessa, M., Chouaibi, M., Ferrari, G., Donsì, F., and Hamdi, S. 2014. Assessment of emulsifying ability of almond gum in comparison with gum arabic using response surface methodology. Food Hydrocolloids 37:49-59.

Mancero-Castillo, D., Beckman, T. G., Harmon, P. F., and Chaparro, J. X. 2018. A major locus for resistance to *Botryosphaeria dothidea* in *Prunus.* Tree Genet. Genomes 14:26.

Martin, J. A., Solla, A., Woodward, S., and Gil, L. 2007. Detection of differential changes in lignin composition of elm xylem tissues inoculated with *Ophiostoma novo-ulmi* using Fourier transform-infrared spectroscopy. For. Pathol. 37:187-191.

Massonnet, M., Morales-Cruz, A., Figueroa-Balderas, R., Lawrence, D. P., Baumgartner, K., and Cantu, D. 2018. Condition-dependent co-regulation of genomic clusters of virulence factors in the grapevine trunk pathogen *Neofusicoccum parvum.* Mol. Plant Pathol. 19:21-34.

Miedes, E., Vanholme, R., Boerjan, W., and Molina, A. 2014. The role of the secondary cell wall in plant resistance to pathogens. Front. Plant Sci. 5:358.

Moral, J., Morgan, D., and Michailides, T. J. 2019a. Management of Botryosphaeria canker and blight diseases of temperate zone nut crops. Crop Prot. 126:104927.

Moral, J., Morgan, D., Trapero, A., and Michailides, T. J. 2019b. Ecology and epidemiology of diseases of nut crops and olives caused by Botryosphaeriaceae fungi in California and Spain. Plant Dis. 103:1809-1827.

Morales-Cruz, A., Amrine, K. C. H., Blanco-Ulate, B., Lawrence, D. P., Travadon, R., Rolshausen, P. E., Baumgartner, K., and Cantu, D. 2015. Distinctive expansion of gene families associated with plant cell wall degradation, secondary metabolism, and nutrient uptake in the genomes of grapevine trunk pathogens. BMC Genomics 16:469.

Morris, H., Hietala, A. M., Jansen, S., Ribera, J., Rosner, S., Salmeia, K. A., and Schwarze, F. W. M. R. 2020. Using the CODIT model to explain secondary metabolites of xylem in defence systems of temperate trees against decay fungi. Ann. Bot. (Lond.) 125:701-720.

Morrison, J. C., Labavith, J. M., and Greve, L. C. 1987. The role of ethylene in initiating gum duct formation in almond fruit. J. Am. Soc. Hortic. Sci. 112:364-367.

Olien, W. C., and Bukovac, M. J. 1982. Ethephon-induced gummosis in sour cherry (*Prunus cerasus* L.): I. Effect on xylem function and shoot water status. Plant Physiol. 70:547-555.

Olmo, D., Armengol, J., León, M., and Gramaje, D. 2016. Characterization and pathogenicity of Botryosphaeriaceae species isolated from almond trees on the island of Mallorca (Spain). Plant Dis. 100:2483-2491.

Pearce, R. B. 1996. Antimicrobial defences in the wood of living trees. New Phytol. 132:203-233.

Pouzoulet, J., Scudiero, E., Schiavon, M., and Rolshausen, P. E. 2017. Xylem vessel diameter affects the compartmentalization of the vascular pathogen *Phaeomoniella chlamydospora* in grapevine. Front. Plant Sci. 8:1442.

Prado, E., and Demarco, D. 2018. Laticifers and secretory ducts: Similarities and differences. In: Ecosystem Services and Global Ecology. IntechOpen, London, U.K.

Ralph, J., Lapierre, C., and Boerjan, W. 2019. Lignin structure and its engineering. Curr. Opin. Biotechnol. 56:240-249.

Ralph, S. A., Ralph, J., and Landucci, L. L. 2009. NMR Database of Lignin and Cell Wall Model Compounds. www.glbrc.org/databases_and_software/nmrdatabase/

Rolshausen, P. E., Greve, L. C., Labavitch, J. M., Mahoney, N. E., Molyneux, R. J., and Gubler, W. D. 2008. Pathogenesis of *Eutypa lata* in grapevine: Identification of virulence factors and biochemical characterization of cordon dieback. Phytopathology 98:222-229.

Ruzin, S. E. 1999. Plant Microtechnique and Microscopy. Oxford University Press, New York.

Saniewski, M., Miyamoto, K., and Ueda, J. 1998. Methyl jasmonate induces gums and stimulates anthocyanin accumulation in peach shoots. J. Plant Growth Regul. 17:121-124.

Saniewski, M., Ueda, J., Miyamoto, K., Horbowicz, M., and Puchalski, J. 2006. Hormonal control of gummosis in Rosaceae. J. Fruit Ornam. Plant Res. 14:137-144.

Sattler, S., and Funnell-Harris, D. 2013. Modifying lignin to improve bioenergy feedstocks: Strengthening the barrier against pathogens? Front. Plant Sci. 4:70.

Serpe, M. D., and Nothnagel, E. A. 1999. Arabinogalactan-proteins in the multiple domains of the plant cell surface. Adv. Bot. Res. 30:207-289.

Shigo, A. L. 1984. Compartmentalization: A conceptual framework for understanding how trees grow and defend themselves. Annu. Rev. Phytopathol. 22:189-214.

Slippers, B., Crous, P. W., Denman, S., Coutinho, T. A., Wingfield, B. D., and Wingfield, M. J. 2004. Combined multiple gene genealogies and phenotypic characters differentiate several species previously identified as *Botryosphaeria dothidea.* Mycologia 96:83-101.

Slippers, B., and Wingfield, M. J. 2007. Botryosphaeriaceae as endophytes and latent pathogens of woody plants: diversity, ecology and impact. Fungal Biol. Rev. 21:90-106.

Sluiter, A. 2008. Determination of Structural Carbohydrates and Lignin in Biomass: Laboratory Analytical Procedure (LAP); Issue Date: 7/17/2005. Technical Report 16.

Sohrabi, M., Mohammadi, H., León, M., Armengol, J., and Banihashemi, Z. 2020. Fungal pathogens associated with branch and trunk cankers of nut crops in Iran. Eur. J. Plant Pathol. 157:327-351.

Úrbez-Torres, J. R. 2011. The status of Botryosphaeriaceae species infecting grapevines. Phytopathol. Mediterr. 50:S5-S45.

Vega-Muñoz, I., Duran-Flores, D., Fernández-Fernández, Á. D., Heyman, J., Ritter, A., and Stael, S. 2020. Breaking bad news: Dynamic molecular mechanisms of wound response in plants. Front. Plant Sci. 11:610445.

Wu, S.-W., Kumar, R., Iswanto, A. B. B., and Kim, J.-Y. 2018. Callose balancing at plasmodesmata. J. Exp. Bot. 69:5325-5339.

Yelle, D. J., Ralph, J., and Frihart, C. R. 2008. Characterization of nonderivatized plant cell walls using high-resolution solution-state NMR spectroscopy. Magn. Reson. Chem. 46:508-517.

Zhang, G., Zhao, F., Chen, L., Pan, Y., Sun, L., Bao, N., Zhang, T., Cui, C.-X., Qiu, Z., Zhang, Y., Yang, L., and Xu, L. 2019. Jasmonate-mediated wound signalling promotes plant regeneration. Nat. Plants 5:491-497.

Zlatković, M., Keča, N., Wingfield, M. J., Jami, F., and Slippers, B. 2016. Botryosphaeriaceae associated with the die-back of ornamental trees in the Western Balkans. Antonie van Leeuwenhoek 109:543-564.